Research Square

Preprints are preliminary reports that have not undergone peer review.
They should not be considered conclusive, used to inform clinical practice,
or referenced by the media as validated information.

Bacterial Preconditioning Differentially Reshapes Neuronal Responses to Intermittent and Continuous Hypoxia-Like Stress

Ariana Leaño-Hinojosa
Complutense University of Madrid
Juan Lombardo-Hernandez
Complutense University of Madrid
Javier Benitez-Cruz
Complutense University of Madrid
Ivana Rapetta
Complutense University of Madrid
Maria Teresa García-Esteban
Complutense University of Madrid
Antonio Murciano-Cespedosa
Complutense University of Madrid
Carmen Juan-Llamas
Complutense University of Madrid
Mari Paz Serrano-Regal
Complutense University of Madrid
Stefano Geuna
University of Turin, Ospedale San Luigi
Luca Cocolin
University of Turin
Celia Herrera-Rincon
ceherrer@ucm.es

Complutense University of Madrid

Research Article

Keywords: Model hypoxia, L. plantarum, preventive treatment, neurobacterial interaction, microbiome, gut bacteria, vascular dementia, bioelectricity

Posted Date: November 10th, 2026

DOI: https://doi.org/10.21203/rs.3.rs-11432235/v1

License: This work is licensed under a Creative Commons Attribution 4.0 International License.
Read Full License

Additional Declarations: No competing interests reported.

Abstract

The microbiota–gut–brain axis exposes the nervous system to microbial information, but whether such exposure becomes part of the biological history that shapes later neuronal stress responses remains unknown. Here, we tested whether transient direct exposure to live *Lactiplantibacillus plantarum* (*L. plantarum*) alters how differentiated B35 neuronal cells subsequently respond to hypoxia-like metabolic stress. We compared two trajectories combining chemical HIF stabilization with nutrient restriction: an intermittent, sublethal condition with recovery periods (MHX), relevant to recurrent vascular insufficiency, and a continuous severe condition (SHX). These trajectories generated distinct structural, metabolic and transcriptional states. Prior *L. plantarum* exposure was associated with higher MTT-derived metabolic viability after MHX but not SHX, and induced broader transcriptional reorganization under MHX (167 versus 64 differentially expressed genes), engaging signaling and cytoskeletal programs together with pathways linked to negative regulation of apoptosis and oxidative-stress-induced cell death. Only one bacterially responsive gene was shared between the two stress trajectories. Thus, *L. plantarum* did not impose a fixed neuroprotective program. Instead, prior microbial exposure acted as a biological input whose consequences depended on the subsequent stress trajectory. These findings establish neuron–bacteria communication as history-dependent and define an adaptive range in which microbial signals can influence neuronal responses before metabolic stress becomes overwhelming—a principle relevant to preventive intervention during recurrent vascular stress.

INTRODUCTION

Vascular cognitive impairment and dementia (VCID) comprise a spectrum of conditions characterized by progressive brain dysfunction, with vascular dementia (VD) representing its most severe form[1]. As the second leading cause of cognitive impairment worldwide after Alzheimer's disease (AD), VD constitutes a major and growing socio-health burden associated with population ageing[2,3]. Notably, its mortality rate is up to 60% higher than that of other dementias, largely due to its strong association with cardiovascular and metabolic comorbidities[4]. Despite its prevalence and impact, VD remains comparatively understudied relative to AD, limiting the development of effective therapeutic strategies[1].

At the cellular level, VD is characterized by sustained reductions in oxygen and nutrient availability, leading to progressive neuronal dysfunction. In contrast to acute neurological insults, this process unfolds gradually through cumulative and often subclinical stress, disrupting neuronal metabolism, synaptic integrity, and survival[2]. This progressive trajectory implies the existence of intermediate states between physiological function and irreversible damage, in which neuronal responses may remain adaptive and potentially reversible. However, these transitional states are poorly defined experimentally. While several modifiable risk factors have been identified at midlife, interventions at later stages—when VCID is most prevalent—have shown limited efficacy[5], emphasizing the need to identify early mechanisms of vulnerability and resilience.

Despite the substantial disease burden, therapeutic progress in VD has been limited, and no FDA-approved treatments are currently available[1]. Existing approaches largely rely on strategies extrapolated from cardiovascular disease or the use of acetylcholinesterase inhibitors, with uncertain efficacy in this context[6]. This limitation reflects, in part, a fundamental gap in experimental modelling. Most *in vitro* systems rely on acute or extreme hypoxic paradigms that fail to capture the progressive nature of chronic oxygen deprivation. As a result, critical windows of early neuronal adaptation—where intervention may be most effective—remain largely unexplored. Developing experimental platforms capable of modelling graded hypoxic stress, distinguishing between mild (adaptive) and severe (maladaptive) regimes, is therefore essential to uncover mechanisms of neuronal resilience and identify novel therapeutic targets.

More broadly, cellular responses to environmental challenges depend not only on the nature of the perturbation itself, but also on the biological history of the responding system. Preconditioning studies have demonstrated that prior sublethal perturbations can alter responses to subsequent injury through extensive molecular and transcriptional reprogramming [7–9]. Such findings indicate that the effect of a biological signal may become apparent not only through its immediate consequences, but also through the way in which it modifies the response to a later challenge. Microbial products have also been investigated as cellular preconditioning inputs, including *L. plantarum* supernatant used to precondition bone marrow-derived mesenchymal stem cells for administration in a rat model of chronic restraint stress[10]. Whether microbial interactions can similarly influence subsequent neuronal stress trajectories remains largely unexplored.

The microbiota–gut–brain axis provides a particularly relevant context in which to address this question. Microbial communities and their molecular products can influence nervous-system physiology through immune, metabolic, endocrine and neural routes[11–13]. The intestinal microbiota, largely composed of gut bacteria, regulates systemic processes such as inflammation and metabolic homeostasis and exerts a significant influence on the central nervous system (CNS)[14]. Dysbiosis has been associated not only with gastrointestinal disorders[15,16] but also with neurological and psychiatric conditions, including cognitive decline and dementia[14,17]. Emerging evidence further suggests that microbiota composition can influence the brain's response to hypoxic stress by modulating oxidative balance, inflammatory pathways, and cognitive outcomes[18]. Within this context, psychobiotics—particularly probiotic strains—have gained increasing attention for their ability to modulate gut–brain communication and promote neuronal health[4,19,20]. Among them, *Lactiplantibacillus plantarum* (*L. plantarum*) has been associated with improvements in cognitive function, neuronal plasticity, and inflammatory balance[21–27]. However, most studies have focused on systemic or indirect mechanisms, leaving unresolved whether—and critically, through which mechanisms—bacterial exposure can directly modulate intrinsic neuronal responses to stress, particularly when applied prior to the onset of cellular damage, as a potential strategy to influence early adaptive responses.

Direct neuron–bacteria interactions provide a reductionist framework to investigate how microbial signals influence intrinsic neuronal physiology. Our previous work demonstrated that live *L. plantarum* can interact directly with neuronal membranes and rapidly modulate calcium dynamics, synaptic-associated proteins, and transcriptional programs in primary cortical neuronal cultures[27]. Complementary evidence has linked bacterial products to hypoxic signaling. Jeong et al. (2024) demonstrated that *L. plantarum* K8 lysates attenuate HIF1α accumulation and hypoxia-responsive gene expression under chemically induced hypoxic conditions [28]. However, in that experimental paradigm, bacterial products remained present during the hypoxic challenge. Whether a preceding interaction with live bacteria can influence neuronal responses to a later metabolic insult, after bacterial removal, remains unresolved. Moreover, it is unclear whether such modulation depends on the nature and severity of the subsequent challenge. Here, we address these questions by considering bacterial exposure not simply as an immediate stimulus, but as a prior biological input whose consequences may depend on the subsequent state and environmental conditions of the receiving neuronal system. This approach places the temporal sequence of microbial interactions at the center of neuron–bacteria communication.

We hypothesized that a transient interaction with live gut bacteria could influence subsequent neuronal responses to metabolic stress, with the nature and magnitude of this modulation depending on the trajectory of the later challenge. To investigate this, differentiated B35 neuronal cells were exposed to live *L. plantarum* for eight hours, followed by a bacterial removal step before the induction of two distinct hypoxia-like metabolic stress regimens: an intermittent condition incorporating repeated recovery periods (MHX) and a continuous severe condition (SHX). Both paradigms combined chemically induced HIF stabilization with glucose and pyruvate restriction. By integrating morphological and immunofluorescence analyses with metabolic activity measurements and RNA sequencing, we investigated whether prior bacterial exposure differentially influences neuronal responses across these distinct stress conditions. Rather than evaluating *L. plantarum* as a uniformly neuroprotective agent, our study addresses a broader question: whether the biological consequences of neuron–bacteria communication depend on the history of microbial exposure and the subsequent environmental challenges encountered by the receiving neuronal system.

MATERIAL AND METHODS

Mild and Severe Ischemia–Hypoxia Model in B35 Neurons

The rat neuroblastoma-derived B35 cell line (ATCC, CRL–2754; LGC Standards, Spain) was used as the neuronal model. Cells were cultured in DMEM medium (Fisher Scientific 11995040) supplemented with 10% fetal bovine serum (FBS, Corning MT 35-010-CV) and 1% penicillin/streptomycin (Pen/Strep; Fisher Scientific 15140122) at 37°C and 5% CO_2. Upon reaching 80–90% confluence, cells were trypsinised (0.25% trypsin-EDTA) and seeded onto plates coated with Poly-D-Lysine (PDL; 50 µg/mL, Thermo Fisher A3890401) at a density of 0.5×10^5 cells/cm². After 12 h of adhesion, differentiation was induced by

replacing the medium with Neurobasal Plus (NB+; Fisher Scientific 21103049) supplemented with 2% B27, 0.25% GlutaMAX, 1% Pen/Strep, and 10 µM all-trans retinoic acid (ATRA; Sigma Aldrich R2625-50). Following a 5-day differentiation period, neurons were either fixed for morphological analysis or subjected to Ischemia–hypoxia conditions. Both mild (MHX) and severe (SHX) models were induced using a combined chemical hypoxia and nutrient restriction paradigm (Fig. 1A). Specifically, cells were exposed to 100 µM cobalt chloride ($CoCl_2$; Sigma-Aldrich, C8661) in glucose- and sodium pyruvate-free Neurobasal medium (NB−; Fisher Scientific, A2477501) supplemented with 1% Pen/Strep. This condition is hereafter referred to as restricted medium (RM). For the severe Ischemia–hypoxia (SHX) model, neurons were continuously maintained in RM for 48 h at 37°C and 5% CO_2. For the mild Ischemia–hypoxia (MHX) model, several exposure paradigms were initially tested to optimize reproducibility and stability of the neuronal response (Suppl. Fig. S1A). The final protocol, selected based on robustness and consistency across experiments, consisted of cyclic exposure to RM for a total duration of 72 h, with daily cycles of 8 h under RM followed by 16 h of reperfusion in standard differentiation medium (NB+ supplemented with 2% B27, 0.25% GlutaMAX, and 1% Pen/Strep).

Neuronal Viability: MTT Assay

Neuronal viability was assessed using a colorimetric assay based on the reduction of MTT (3-(4,5-dimethylthiazol-2-yl)-2,5-diphenyltetrazolium bromide; Thermo Scientific, M6494). MTT was added to each well at a final concentration of 0.5 mg/mL from a 5 mg/mL stock solution prepared in PBS, and cells were incubated for 1 h at 37°C in a 5% CO_2 atmosphere. Following incubation, the medium was carefully removed and 200 µL of dimethyl sulfoxide (DMSO; Merck, d8418-50) was added to solubilize the formazan crystals. Absorbance was measured at 590 nm using a microplate reader (Heales MB-580). Optical density (OD) values were used as an indicator of cellular metabolic activity. Cell viability was expressed as a percentage relative to untreated control neurons, which were set to 100%. This assay was used to compare neuronal viability across hypoxic conditions (MHX vs SHX) and to assess the effect of bacterial preconditioning on neuronal survival within each condition.

Immunofluorescence Assay and Microscopy

At the end of each hypoxia protocol, B35 cells were fixed using a two-step paraformaldehyde (PFA; Thermo Fisher Scientific, J19943-K2) fixation procedure to minimize cell detachment. Briefly, 100 µL of 4% PFA in PBS was added directly to the culture medium and incubated for 2 min (37°C, 5% CO_2). Subsequently, the medium was replaced with fresh 4% PFA and samples were fixed for an additional 20 min at room temperature (RT). After two washes with PBS, samples were maintained overnight (ON) at 4°C. Cells were then permeabilized with 0.1% Triton X-100 in PBS for 30 min at RT, followed by blocking in 10% normal goat serum (NGS; Sigma-Aldrich S26-M) in 0.1% PBS–Triton for 30 min at RT. Samples were then incubated ON at 4°C with primary antibodies against βIII-TUBULIN (TUBB3), hypoxia-inducible factor 1-alpha (HIF1A), Synapsin I (SYN1), and pCREB (see Suppl. Table S1 for details), diluted in 1% bovine serum albumin (BSA; VWR 9048-46-8) and 1% NGS in 0.1% PBS–Triton. Following three PBS

washes, appropriate Alexa Fluor-conjugated secondary antibodies (anti-mouse and anti-rabbit, 1:500; Invitrogen) were added and incubated for 2 h at RT with agitation. Nuclear staining was performed using DAPI (1:5000 in PBS; Fisher Scientific, 62248) for 5–10 min. For sample visualisation, an inverted fluorescence microscope Leica DM IRB was used, equipped with filters A, I3, GFP, and N2.1: blue (488 nm, 20 mW), green (552 nm, 20 mW), and red (638 nm, 30 mW). Image acquisition was performed by systematic random sampling, selecting at least three distinct fields per well (3 images × 3 technical replicates × 3 biological replicates; N = 9). All images within each experiment were captured on the same day using identical acquisition and processing settings to ensure comparability of fluorescence intensity measurements.

Image Processing and Quantitative Analysis

Quantitative analysis of microscopy images was performed using ImageJ/Fiji software (National Institutes of Health, Bethesda, MD, USA). A standardized analysis pipeline was applied to all images, with variations only in the specific parameters quantified depending on the marker. First, background subtraction was performed to reduce non-specific signal. A fluorescence threshold was then applied to segment marker-positive regions, ensuring that subsequent measurements were restricted to pixels exceeding this threshold. Both area and fluorescence intensity measurements were therefore calculated exclusively within these segmented regions. Marker-specific analysis was subsequently conducted. For TUBB3 and SYN1, the marker-positive area was quantified and normalized to the number of cells per field, estimated by counting DAPI-stained nuclei. In the case of HIF1A, the mean fluorescence intensity was calculated. Finally, for pCREB, mean fluorescence intensity within marker-positive regions was measured, as this parameter reflects relative changes in transcription factor levels per nucleus across experimental conditions. Nuclei quantification was performed using DAPI staining following an analogous workflow, including background subtraction, thresholding, and particle counting to determine the number of nuclei per field. For the analysis of neuronal morphometry and branching analysis in TUBB3-labelled images, following background subtraction, images were enhanced for contrast (0.35% saturated pixels) and subjected to noise reduction (radius = 1–2 px) before segmentation using an automatic thresholding method (Otsu). The resulting binary images were then skeletonized (Skeletonize) to obtain a one-pixel-wide representation of the neuronal network. Skeletonized images were analyzed using the Analyze Skeleton (2D/3D) plugin to quantify the total branch length per field of view. This parameter was used as a proxy for neuronal network complexity and compared across experimental conditions. The analysis was performed consistently across all images, and for each condition, values were averaged across all analysed fields.

Lactiplantibacillus plantarum Strain and Growth Conditions

The bacterial strain *Lactiplantibacillus plantarum* O2T60C (*L. plantarum*) was cultured in de Man, Rogosa and Sharpe medium (MRS; Oxoid CM0359B) and stored at − 80°C in the same medium supplemented with 20% glycerol (v/v; Sigma-Aldrich). For experimental use, bacteria were recovered from frozen stocks, streaked onto MRS agar plates, and a single isolated colony was used to inoculate liquid MRS

medium. Cultures were incubated for 24 h under standard growth conditions. Bacterial growth kinetics were previously characterized [27], and to ensure reproducibility in neuron–bacterium interaction assays, bacteria were consistently harvested at the early stationary phase, corresponding to approximately 18 h of growth for *L. plantarum*.

Neuron–Bacteria Interaction: Bacterial Preconditioning with Lactiplantibacillus plantarum

To assess whether prior bacterial exposure modifies subsequent neuronal stress responses, differentiated B35 cells were exposed to *L. plantarum* for 8 h before the induction of hypoxia-like metabolic stress (Fig. 3A). After 18 h of growth, bacterial suspensions were adjusted to an optical density of OD_{600} ≈ 0.3, centrifuged (2000 × g, 10 min, RT), and the resulting pellet was resuspended in antibiotic-free Neurobasal Plus medium (NB+). To facilitate adaptation to the neuronal culture conditions, bacteria were incubated in NB + for 10 min at RT prior to the interaction assay. Before bacterial addition, neuronal cultures were washed with PBS to remove residual antibiotics. Bacteria were then added to the neuronal culture on day 5 post differentiation at a multiplicity of infection (MOI) of 10 (i.e., 10 colony-forming units per neuron). Neuron–bacteria co-interaction cultures were maintained for 8 h at 37°C in a humidified atmosphere containing 5% CO_2. Following the 8 h co-incubation period, bacteria were fully removed, and neuronal cultures were subsequently subjected to either the MHX or SHX stress regimen described above.

RNA Extraction and Gene Expression Analysis (qPCR)

For quantitative real-time PCR (qPCR) and RNA-sequencing (RNA-seq) analyses, neuronal samples were collected immediately after completion of the MHX and SHX treatments. Culture medium was removed from each well, and cells were washed twice with PBS at RT. Subsequently, 400 µL of cold PBS (4°C) was added to each well, and cells were detached by gentle scraping for approximately 30 s. The resulting cell suspension was collected and immediately placed on ice. Samples were stored at − 80°C for up to 7 days prior to RNA extraction. RNA isolation was performed using the TRIzol™ Plus RNA Purification Kit (Invitrogen™), following the manufacturer's instructions. RNA concentration and purity were assessed using a NanoDrop One spectrophotometer (Thermo Fisher Scientific).

For qPCR analyses, complementary DNA (cDNA) was synthesized from 500 ng of total RNA using the PrimeScript™ RT Master Mix (Perfect Real Time) Kit (Takara Bio Inc.) in a final reaction volume of 10 µL. qPCR reactions were carried out using the TaqMan™ Fast Advanced Master Mix (Applied Biosystems), with 1:10 dilutions of cDNA and specific TaqMan Assays (Thermo Fisher Scientific) for each target gene, specifically *Fos*, *Hif1a*, and *Syn1* (Suppl. Table S2), according to the manufacturer's protocol. Reactions were run on a QuantStudio 7 Real-Time PCR System (Applied Biosystems) in 384-well format, with the following thermal cycling conditions: 95°C for 20 s, followed by 40 cycles of 95°C for 1 s and 60°C for 20s.Data collection and analysis were carried out using the QuantStudio Real-Time PCR Software v1.3. Amplification curves and threshold cycle (Ct) values, indicating the cycle at which fluorescence surpasses the threshold, were used for relative quantification using the ΔΔCt method. Gene expression

was normalized to the reference gene glyceraldehyde-3-phosphate dehydrogenase (GAPDH) and fold changes were expressed as RQ values relative to the control condition. The entire study comprised three independent biological replicates ($n = 3$ plates) for each treatment set (SHX and MHX). Within each plate, tissue from six wells per condition was pooled in pairs to yield three samples, resulting in a total of 9 treatment and 9 control pooled samples per set. RNA extraction and qPCR analysis was performed at the Genomics Unit of the Research Support Center (CAI) of Biological Techniques, Faculty of Biological Sciences, Complutense University of Madrid (UCM, Spain).

RNA-seq and transcriptomics analyses

All RNA-seq analyses, including quality control, differential gene expression analysis, and downstream functional analyses, were performed by Novogene Europe (GmbH, 82152 Planegg, Germany) using their standard bioinformatics workflow and the NovoMagic analysis platform (2023; https://eu-magic.novogene.com/#/.) Total RNA samples, previously extracted and stored at − 80°C, were shipped on dry ice. All samples passed quality control assessments, including RNA concentration, purity, and integrity, evaluated using an Agilent 5400 system.

Library preparation and Sequencing

Messenger RNA (mRNA) was enriched from total RNA using poly-T oligo-attached magnetic beads. Following fragmentation, first-strand cDNA synthesis was performed using random hexamer primers, followed by the second strand synthesis. Libraries were constructed through end repair, A-tailing, adapter ligation, size selection, amplification, and purification. For strand-specific libraries, second-strand synthesis was carried out using dUTP instead of dTTP, followed by USER enzyme digestion to preserve strand information. Library quality and concentration were assessed using Qubit, real-time PCR, and Bioanalyzer analysis. Libraries were pooled and sequenced on an Illumina platform using a sequencing-by-synthesis approach.

Data Processing and Quality Control

Raw sequencing reads (FASTQ format) were processed using fastp to remove adapters, reads containing poly-N sequences, and low-quality reads. Quality metrics, including Q20, Q30, and GC content, were calculated. All downstream analyses were performed using high-quality clean reads.

Read Alignment and Transcript Assembly

Clean reads were aligned to the reference genome using HISAT2 (v2.2.1), enabling splice-aware alignment. Transcript assembly and quantification were performed using StringTie (v2.2.3) in a reference-guided approach, allowing identification of known and novel transcript isoforms.

Gene Expression Quantification

Gene-level read counts were obtained using feature Counts (v2.0.6), and expression levels were normalised as fragments per kilobase of transcript per million mapped reads (FPKM), accounting for both gene length and sequencing depth.

Differential Gene Expression Analysis

Differential expression analysis between experimental conditions was performed using the DESeq2 R package (v1.42.0), based on a negative binomial distribution model. P-values (p) were adjusted for multiple testing using the Benjamini–Hochberg procedure. For analyses, genes were selected using a nominal p-value ≤ 0.05 and $|\log_2$ fold change$| \geq 1$. These gene lists were used for descriptive comparisons and functional categorization; adjusted p-values are provided in the supplementary datasets. To further characterize the transcriptional responses, representative genes with identifiable gene symbols were selected from the gene lists meeting the predefined nominal differential-expression thresholds. Functional annotations were retrieved from the Rat Genome Database. Selected genes, together with their corresponding $\log_2$ fold changes, nominal p-values, gene types, and functional descriptions, are presented in Supplementary Tables S3–S5. The complete lists of genes meeting the selection criteria for each experimental comparison are provided in Annex Data S1–S4.

Functional Enrichment Analysis

Gene Ontology (GO) and Kyoto Encyclopedia of Genes and Genomes (KEGG) enrichment analyses were performed using the cluster Profiler R package (v4.8.1). Pathways with nominal p-values ≤ 0.05 were considered for functional interpretation. GO overrepresentation analysis was additionally performed using the PANTHER Overrepresentation Test, focusing on Biological Process and Molecular Function annotations, with annotated Rattus norvegicus genes as the reference background. Fisher's exact test was applied, with multiple-testing correction using the false discovery rate (FDR) method. Additionally, Gene Set Enrichment Analysis (GSEA) was performed using the Broad Institute GSEA software to identify coordinated changes in predefined gene sets based on genes ranked according to differential expression between experimental conditions. GO and KEGG gene sets were evaluated independently.

Functional classification of DEGs into major biological categories

DEGs were analyzed using a custom workflow implemented in *R*, comprising four sequential steps: (i) functional annotation, (ii) multi-label functional classification and visualization, (iii) statistical comparison between upregulated and downregulated genes within each contrast, and (iv) statistical comparison across experimental contrasts. Functional annotation was primarily performed using the *Ensembl* database via the *biomaRt* R package. Gene annotation queries were performed in batches to improve stability. Retrieved fields included gene symbol, description, gene biotype, GO identifiers, GO term names, and GO namespaces. Annotations were summarized at the gene level, retaining representative descriptions and aggregating GO terms, with explicit separation of biological process terms. Annotated gene lists were subjected to multi-label functional classification using a keyword-based approach. Relevant annotation fields were concatenated into a unified text string per gene and

interrogated using regular expressions against a manually curated dictionary of biological categories. Genes lacking valid symbols were excluded to minimize poorly characterized entries. Functional categories included synapse, bioelectrical signaling, transcriptional regulation, signaling, metabolism, mitochondrial/oxidative stress, hypoxia/ischemia, transport, inflammation, immune/stress response, cell cycle/proliferation, cell death/autophagy, neurodegeneration, cytoskeleton/adhesion, RNA/translation, and others. (To check the whole filtering terms, see Suppl. Text S4). The bioelectrical signaling category was operationally defined using annotations related to ion channels, membrane excitability, membrane potential regulation, ion transport, and metal-ion homeostasis (Supplementary Text S4). Accordingly, this annotation-based classification captures genes potentially associated with ionic and membrane-related processes but does not provide direct evidence of changes in neuronal electrical activity. Classification was performed in a multi-label framework, allowing genes to be assigned to multiple categories. Category-level summaries were computed as gene counts and proportions relative to annotated genes, as well as relative to total category assignments. To assess differential enrichment, functional category representation was compared between upregulated and downregulated genes within each contrast, as well as across experimental conditions. Statistical significance was evaluated using binomial logistic regression and Fisher's exact test, based on gene membership within each category. Odds ratios (OR), 95% confidence intervals, and p-values were calculated and adjusted for multiple testing using the Benjamini–Hochberg method. Results were visualized using forest plots. This framework enabled systematic functional characterization of DEG datasets, capturing the multi-functional nature of genes while providing robust statistical assessment of category enrichment across conditions.

Clustering Analysis according to hallmark gen list

To evaluate the transcriptional organization of samples according to hypoxic severity and bacterial treatment, unsupervised hierarchical clustering was performed using predefined gene sets relevant to hypoxia and bacteria-induced neuronal responses. Hypoxia-related analyses included gene sets associated with hypoxia-inducible factor-1α (HIF-1α) signaling (GO:0097411), response to hypoxia (GO:0001666), and chronic cerebral hypoperfusion (DOID:9007970). To assess the transcriptional effects of bacterial treatment under mild and severe hypoxia, additional gene sets related to response to bacterium (GO:0009617), response to nutrient levels (GO:0031667), inflammatory response (GO:0006954), and negative regulation of apoptotic process (GO:0043066) were analyzed. For each gene set, normalized expression values were extracted, and bidirectional hierarchical clustering of genes and samples was performed, with samples represented as columns. These analyses were used to determine whether functionally defined transcriptional profiles could discriminate between mild and severe hypoxia and between bacteria-treated and untreated samples within each hypoxic condition.

Statistical Analysis

Statistical analyses were performed according to the nature of the data and the structure of the experimental design. Prior to analysis, continuous variables were assessed for normality using the Shapiro–Wilk test and for homogeneity of variances using Levene's test. For assays involving comparisons across three groups (Control -CTRL-, MHX, and SHX), including MTT and

immunofluorescence-derived metrics (e.g., TUBB3 area and DAPI-based cell count), group differences were evaluated using one-way analysis of variance (ANOVA) when parametric assumptions were met. When these assumptions were violated, the non-parametric Kruskal–Wallis test was applied. In both cases, appropriate post hoc multiple comparison tests were performed (Tukey's test for ANOVA or Dunn's test for non-parametric analysis), with adjustment for multiple testing. For pairwise comparisons (e.g., qPCR analyses between the two treatments), statistical significance was assessed using the Student's t-test or, when normality assumptions were not satisfied, the Mann–Whitney U test. For immunofluorescence data with repeated measurements (multiple fields per biological replicate), group differences were analysed using population-averaged generalized estimating equation (GEE) models, assuming a Gaussian distribution with an identity link function and an exchangeable correlation structure to account for intra-sample correlation. The significance of fixed effects was evaluated using Wald χ^2 tests. All analyses were conducted using GraphPad Prism (v10) and Stata (version XVI). Unless otherwise stated, each experimental condition included at least three independent biological replicates and a minimum of three technical replicates. Results are presented as mean ± standard error of the mean (SEM). Statistical significance was set at p-value (p) < 0.05. Significance levels are indicated as follows: $p < 0.05$ (*), $p < 0.01$ (**), $p < 0.001$ (***); and $p < 0.0001$ (****).

RESULTS

A graded hypoxia model defines an intermediate neuronal state between homeostasis and severe degeneration

To establish an *in vitro* model capable of capturing graded neuronal responses to hypoxic stress [29], we developed a chamber-independent paradigm combining chemical hypoxia with nutrient restriction. This approach enabled the distinction between severe hypoxia (SHX), representing maximal neuronal damage, and mild hypoxia (MHX), modelling sustained but sublethal stress associated with chronic intermittent oxygen deprivation (Fig. 1A; see also Suppl. Text S1 and Fig. S1A for optimization details). To validate the robustness of the experimental design, neuronal responses to MHX and SHX were assessed through complementary analyses of viability and morphology. (Fig. 1B-F).

MTT assays revealed a significant reduction in cellular viability in both hypoxia conditions compared to CTRL group (differentiated and untreated neurons in normoxia), with SHX inducing the strongest effect and MHX displaying an intermediate phenotype (one-way ANOVA $p < 0.0001$; CTRL = 1.000 ± 0.01498 a.u; SHX = 0.5588 ± 0.01971 a.u; MHX = 0.7447 ± 0.02924 a.u; all post hoc comparisons $p < 0.0001$; Fig. 1B). Consistent with these findings, morphological and structural analysis further distinguished the two conditions (Fig. 1C–F). CTRL neurons exhibited typical differentiated morphology, characterized by extensive neuritic extensions and strong intercellular connectivity (Fig. 1C; Suppl. Fig. S1B). In contrast, SHX-treated cells showed pronounced structural disruption, including soma rounding, loss of adhesion, and network disintegration. Notably, MHX induced partial alterations while preserving aspects of neuronal connectivity, consistent with an intermediate damage state. Quantitative analyses reinforced

this phenotype. Neuronal density analysis revealed a graded reduction across conditions, with the lowest cell counts in SHX, intermediate levels in MHX, and highest in CTRL conditions (Kruskal–Wallis, CTRL = 216.5 ± 8.807 DAPI+ nuclei, SHX = 122.6 ± 10.74 DAPI+ nuclei, MHX = 143.9 ± 12.67 DAPI+ nuclei; CTLR–SHX $p < 0.0001$; CTLR–MHX $p < 0.0001$; SHX–MHX $p = 0.1976$; Fig. 1D). Likewise, levels of the neuronal cytoskeletal marker βIII-tubulin (TUBB3) [30] were significantly reduced under SHX, whereas MHX values remained closer to CTRL (Kruskal–Wallis, CTRL = 284,611 ± 15,202 a.u, SHX = 174,654 ± 10,242 a.u, MHX = 263,688 ± 14,087 a.u; CTLR–SHX $p < 0.0001$; CTLR–MHX $p = 0.7368$; SHX–MHX $p < 0.0001$; Fig. 1E). Similarly, total neuritic length was severely compromised in SHX but largely preserved in MHX (Kruskal–Wallis, CTRL = 35,107 ± 1,846 a.u, SHX = 12,737 ± 1,127 a.u, MHX = 34,822 ± 2,095 a.u; CTLR–SHX $p < 0.0001$; CTLR–MHX $p = 0.8925$; SHX–MHX $p < 0.0001$; Fig. 1F).

Together, these results demonstrate that the proposed hypoxia–Ischemia paradigm reliably reproduces distinct levels of neuronal damage, with MHX capturing a controlled intermediate state between homeostasis and severe degeneration, affecting viability, morphology, and cytoskeletal integrity.

Hypoxia severity defines distinct neuronal states with divergent structural and transcriptional programs

To further characterize the neuronal states defined by MHX and SHX, we examined key markers associated with hypoxia, neuronal plasticity, and synaptic integrity using immunofluorescence. HIF1A, a master regulator of the cellular hypoxia response [31,32], showed a clear divergence between conditions. Qualitatively, SHX-treated neurons exhibited rounded morphology, loss of adhesion, and the presence of cellular aggregates with diffuse interconnections, whereas MHX maintained a more preserved cellular architecture with clearly defined neuronal connections (Fig. 2A). Quantitative analysis confirmed significantly higher HIF1A mean expression under SHX compared to MHX (population-averaged GEE, Wald $\chi^2 = 9.46$, $p = 0.0021$; Fig. 2B), consistent with an enhanced hypoxic stress response. Phosphorylated CREB (pCREB), a regulator of activity-dependent transcription and neuronal plasticity [33–35], remained relatively stable across conditions. Qualitative assessment showed comparable signal distribution between MHX and SHX (Fig. 2C), and population-averaged GEE analysis did not identify significant differences (Wald $\chi^2 = 0.01$, $p = 0.93$; Fig. 2D), suggesting preserved baseline activation of this pathway under both hypoxic regimes. In contrast, synapsyn 1 (SYN1), a marker of synaptic integrity [36,37], further distinguished the two conditions. Under SHX, neurons showed reduced SYN1 signal together with disrupted morphology, including loss of adhesion and network fragmentation. By contrast, MHX preserved a more interconnected neuronal network with clearly defined neuritic contacts (Fig. 2E). Quantitative analysis confirmed significantly higher SYN expression under MHX compared to SHX (population-averaged GEE, Wald $\chi^2 = 11.21$, $p = 0.0008$; Fig. 2F), supporting partial preservation of synaptic architecture under mild hypoxia. Consistent with the morphological and protein-level differences, RT-qPCR analysis supported a divergence in transcriptional profiles between conditions. MHX showed higher expression of genes associated with neuronal activity and connectivity, including *c-*

Fos [38–40] and *Syn1*, whereas SHX was characterized by increased *Hif1a* expression (detailed quantitative results are provided in the Suppl. Text S2 and Fig. S2A-C).

To further resolve these differences, we performed RNA sequencing (next-generation sequencing or NGS), to comprehensively characterize the molecular signatures associated with each condition. Unsupervised clustering analysis revealed two clearly separated groups corresponding to MHX and SHX samples (Fig. 2G). Notably, this segregation was maintained even when restricting the analysis to gene sets specifically associated with hypoxia-related pathways, including *Hif1a* signaling (GO 0097411), hypoxia response genes (GO 0001666), and chronic cerebral hypoperfusion signatures (DOID:9007970; Suppl. Fig. S2 D-F), indicating a robust and condition-specific transcriptional organization. Differential expression analysis identified 2,065 genes meeting the predefined thresholds ($|\log_2 FC| \geq 1$, $p \leq 0.05$), of which 1,096 were upregulated and 969 were downregulated in MHX relative to SHX (Fig. 2H; Annex Data S1 for the complete gene list and Supplementary Table S3 for selected annotated genes). Functional categorization (Fig. 2I) revealed that the most represented biological processes included signaling (21%), metabolism, structural organization/adhesion (12.7%), and cell cycle-related processes (11.7%). GO enrichment analysis (Fig. 2J, K) indicated that genes upregulated in MHX were predominantly associated with cell cycle-related and structural processes, whereas genes enriched in SHX were linked to neuronal communication and signaling, particularly ion channel activity and synaptic membrane components. These trends were further supported by categorical analysis (Fig. 2L), which showed significant enrichment of cell cycle/proliferation and structural categories in MHX, alongside a relative depletion of synaptic and signaling-related functions.

Together, these multi-level analyses demonstrate that hypoxia severity defines two distinct neuronal states, in which mild hypoxia preserves structural organisation while engaging a proliferative-associated transcriptional program, whereas severe hypoxia is characterized by structural collapse and a stress-associated signaling signature.

Bacterial preconditioning preserves neuronal viability selectively under mild hypoxia and defines state-dependent transcriptional responsiveness

Having established that our in vitro hypoxia model robustly generates two clearly distinct neuronal states, with divergent morphological and transcriptional profiles, we next investigated whether prior exposure to *L. plantarum* could modulate the neuronal response to subsequent graded hypoxic stress (Fig. 3A). Neurons were pre-exposed to direct bacterial contact for 8 h at a multiplicity of infection (MOI) of 10:1, a condition previously shown to elicit robust phenotypic and transcriptional responses in a similar model [27]. Experimental groups were defined based on hypoxia severity and bacterial exposure, resulting in four conditions: MHX control (MHX-C), MHX with bacterial preconditioning (MHX-B), SHX control (SHX-C), and SHX with bacterial preconditioning (SHX-B).

First, to evaluate the ability of bacterial preconditioning to modulate the neuronal response to subsequent hypoxic exposure, neuronal viability was assessed using the MTT assay. Under severe hypoxia, no significant differences were observed between control and bacteria-preconditioned neurons (Fig. 3B; SHX-C vs SHX-B; $p = 0.8210$), indicating that bacterial preconditioning fails to rescue neuronal viability under high-stress conditions. In contrast, under mild hypoxia (MHX), neurons pre-exposed to *L. plantarum* exhibited significant higher viability compared to control conditions (Fig. 3C; MHX-C vs MHX-B; $p = 0.0045$), demonstrating that bacterial preconditioning enhances neuronal survival under moderate stress.

Next, to determine whether these functional differences were associated with differential transcriptional responses, we performed RNA sequencing across the four experimental conditions (Fig. 3D). Principal component analysis (PCA) revealed that hypoxia severity was the dominant source of transcriptional variance, with samples segregating along PC1 (84.01%) according to MHX and SHX conditions (Suppl. Figure 3A–C). Within each hypoxic regime, bacterial preconditioning induced a separation along PC2 (11.75%). Notably, MHX samples (C and B) showed a clear separation upon *L. plantarum* exposure, indicating preserved transcriptional responsiveness to bacterial contact. In contrast, SHX samples (C and B) remained closely clustered, suggesting markedly reduced transcriptional modulation in response to bacterial preconditioning under severe hypoxia. To further resolve these effects, differential expression analyses were performed within each hypoxic condition, comparing control (C) and bacteria-preconditioned (B) groups.

Under SHX conditions, 64 genes met the predefined differential-expression thresholds ($|\log_2 FC| \geq 1$, $p \leq 0.05$), including 31 upregulated and 33 downregulated genes in SHX-B relative to SHX-C (Fig. 3E, F; Annex Data S2). To further characterize the most responsive transcriptional changes, we extracted the top DEGs showing the highest magnitude of response (Suppl. Table S4). Among the up-regulated genes, the most biologically plausible candidates were associated with lipid and stress-related metabolism, protease regulation, and adaptive signaling, including *Ephx2, Bmp6, Gulo*, and Serpinb1b. In contrast, down-regulated genes included key components of neuronal communication and synaptic organization, such as *Gria1* and *Sparcl1*, together with genes related to membrane trafficking and neurite-associated regulation. Functional classification, GO and GSEA enrichment analyses further supported this pattern, revealing an enrichment of categories related to metabolism and transcriptional regulation under SHX, alongside a relative depletion of processes linked to bioelectrical signaling, synaptic function, and neurodegeneration (Fig. 3G; Suppl. Fig. S3D-F; see Data Appendix S3). Notably, several of the top-ranked DEGs were not canonical neuronal markers, and non-categorized DEGs accounted for up to 11.1% of the total, representing the second most abundant category (Fig. 3F). Together, these findings suggest that under severe hypoxia, bacterial preconditioning elicits a limited and functionally skewed transcriptional response, predominantly characterized by metabolic and stress-adaptive processes rather than neuronal-specific programs.

In contrast, under MHX conditions, bacterial preconditioning was associated with a broader transcriptional response, with 167 genes meeting the predefined differential-expression thresholds

($|\log_2 FC| \geq 1$, $p \leq 0.05$), including 67 upregulated and 100 downregulated genes in MHX-B relative to MHX-C (Fig. 3H,I; Annex Data S3). To further characterize the most responsive transcriptional changes, we extracted the top DEGs with the highest magnitude of response (Suppl. Table S5). Among the most up-regulated DEGs, several candidates were associated with signaling, stimulus detection, cytoskeletal organization, and adaptive cellular responses, including *Htr2a*, *Septin14*, *Tmem74*, *Caps2*, and *Tafa3*. Additional induced genes, such as *Il11*, *Il9r*, *C4bpb*, and *Tigit*, pointed to modulation of cytokine-related and immune-associated pathways. The most down-regulated DEGs included components linked to cellular structure, vesicular trafficking, apoptosis, and synaptic regulation, such as *Marcksl1*, *Bloc1s3*, *Moap1*, *Pspn*, and *C1ql1*.

Functional classification of DEGs, together with GO and GSEA enrichment analyses, further supported that upregulated genes were primarily associated with adaptive immune responses and stimulus detection. Categories such as inflammation and bioelectrical signaling showed a clear bias toward upregulation, whereas processes including transcriptional regulation, metabolic pathways, and neurodegeneration were predominantly downregulated (Fig. 3J; Suppl. Fig. S3G–I; see Data Appendix S5). Notably, GSEA revealed an enrichment of gene sets associated with the negative regulation of cell death (Suppl. Fig. S4, S5), including *negative regulation of intrinsic apoptotic signaling pathway by p53* (GO:1902254) and *negative regulation of oxidative stress–induced cell death* (GO:1903204), together with a decrease in pathways related to the execution phase of apoptosis (GO:1900117). Together, these findings indicate that under mild hypoxia, *L. plantarum* induces a broader and more coordinated transcriptional response compared to severe hypoxia. This response is consistent with preserved neuronal responsiveness to bacterial exposure and involves the activation of signaling, cytoskeletal, and immune-modulatory pathways, alongside a modulation of cell death programs.

Collectively, our results define mild hypoxia as the condition in which bacterial preconditioning can still engage a measurable neuronal transcriptional program, whereas severe hypoxia shifts cells towards a restricted state largely refractory to psychobiotic modulation.

L. plantarum preconditioning reshapes hypoxia-dependent transcriptional programs within a restricted window of neuronal plasticity

After establishing the differential transcriptional responsiveness to bacterial exposure under hypoxic conditions, we next investigated how bacterial presence modulates transcriptional differences between the two hypoxia paradigms. To this end, we performed a comparative analysis of shared and condition-specific DEGs between moderate and severe hypoxia under control conditions (MHX-C vs SHX-C) and following bacterial pre-treatment (MHX-B vs SHX-B) (Fig. 4A). A total of 1,300 DEGs were shared between the two comparisons, representing 62.95% of the 2,065 DEGs detected in MHX-C vs. SHX-C and 59.80% of the 2,174 DEGs detected in MHX-B vs. SHX-B. This substantial overlap highlights the dominant effect of hypoxic severity over bacterial presence in shaping the transcriptional landscape. However, the distribution of shared and exclusive DEGs across functional categories was not uniform. Cell cycle and proliferation categories showed a significant enrichment among shared DEGs (common cell cycle DEGs

= 68.86%, $p < 0.001$), whereas categories such as synaptic function were preferentially enriched among condition-specific genes (common synapse DEGs = 38.28%, $p = 0.002$; Fig. 4B). These findings indicate that hypoxia severity primarily governs proliferation-related pathways, while bacterial presence preferentially modulates signaling and stimulus-response processes.

Having confirmed the differential modulation of hypoxia and bacterial treatment, we next examined DEGs exclusively distinguishing hypoxic conditions in the presence or absence of bacteria. We identified 765 exclusive DEGs in MHX-C vs SHX-C and 874 in MHX-B vs SHX-B, indicating increased transcriptional divergence between hypoxic states upon bacterial exposure. Functional categorization analysis revealed that bacteria-specific DEGs were predominantly associated with transport, cell death, and synaptic processes, along with a significant enrichment in signaling pathways (odds ratio = 1.52, $p = 0.002$). In contrast, DEGs exclusive to control conditions were mainly linked to metabolic processes (odds ratio = 0.69, $p = 0.012$) and mitochondrial activity (odds ratio = 0.66, $p = 0.012$) (Fig. 4C). Together, these results demonstrate that bacterial presence shifts the transcriptional response toward pathways involved in intercellular communication and cell fate regulation.

To further dissect the context-dependent effects of bacterial treatment, we compared its impact under severe hypoxia—where neuronal viability is markedly compromised (SHX-B vs SHX-C)—and moderate hypoxia, which induces partial neuronal impairment (MHX-B vs MHX-C; Fig. 4D). Notably, only one gene, LOC120093785, met the predefined differential-expression thresholds ($|\log_2 FC| \geq 1$, $p \leq 0.05$) in both bacterial comparisons (MHX-B vs MHX-C and SHX-B vs SHX-C; Fig. 4D). This limited overlap suggests that prior *L. plantarum* exposure is associated with largely distinct transcriptional responses depending on the subsequent metabolic stress trajectory, further supporting the context-dependent nature of neuron–bacteria communication. Categorical analysis of DEGs exclusively induced by bacterial treatment within each hypoxic background revealed a bias across most relevant functional categories—including transport, structural organization/adhesion, and signaling—toward stronger dysregulation under moderate hypoxia. In contrast, the non-classified DEGs category showed a relative enrichment under severe hypoxia (Fig. 4E). Notably, moderate hypoxia was associated not only with a global increase in the number of bacteria-induced DEGs across most functional categories, but also with higher absolute log2 fold-change values, indicating a more pronounced transcriptional impact of bacterial treatment under these conditions (Suppl. Fig. S6A, B). Consistently, clustering analysis based on hallmark gene sets, such as response to bacterium (GO:0009617), response to nutrient levels (GO:0031667), inflammatory response (GO: 0006954) or negative regulation of apoptosis (GO:0043066) revealed clear segregation between bacteria-treated and untreated samples under moderate hypoxia, whereas this separation was largely lost under severe hypoxia (Suppl. Fig. S6C-F). Together, these results reinforce the notion that the modulatory capacity of bacteria is largely restricted to non-extreme hypoxic conditions.

Overall, these results demonstrate that hypoxic severity is the primary determinant of the neuronal transcriptional landscape, while bacterial exposure exerts a context-dependent modulatory effect. Notably, *L. plantarum* enhances transcriptional plasticity and promotes functional resilience specifically

under moderate hypoxia, whereas its impact is largely diminished under severe stress conditions. Together, these findings identify a restricted window in which bacterial preconditioning effectively modulates neuronal responses, linking transcriptional reprogramming with improved cellular viability

DISCUSSION

Neuronal stress responses are commonly studied as reactions to isolated insults, although cells encounter each challenge from a state shaped by previous biological interactions. This history dependence is particularly relevant in neurons, whose adaptation to metabolic stress may depend on the sequence as well as the nature of preceding inputs. Here, a transient interaction with *L. plantarum* before hypoxia-like stress modified the subsequent neuronal response according to the trajectory of the challenge. Pre-exposure increased MTT-derived metabolic viability and elicited broad transcriptional reorganization after intermittent sublethal stress (MHX), but did not improve metabolic viability and produced a more restricted transcriptional response after continuous severe stress (SHX). Thus, *L. plantarum* did not impose a fixed neuroprotective program; prior microbial exposure acted as a biological input whose consequences emerged from the state in which the later stress was encountered.

Morphological, metabolic and molecular analyses consistently distinguished the two trajectories. SHX caused extensive loss of cellular adhesion, soma rounding and network disintegration, accompanied by a pronounced decrease in MTT-derived metabolic viability and reduced neuronal and synaptic markers. MHX produced an intermediate metabolic reduction while comparatively preserving TUBB3-positive structures, neuritic length and neuronal interconnections (Fig. 1B–F). Greater HIF1A accumulation under SHX, together with higher SYN1 protein and *Fos* and *Syn1* expression under MHX, further supported the distinction between a severely compromised, stress-dominated state and an intermittent state retaining capacity for cellular reorganization (Fig. 2A–F; Suppl. Fig. S2A–C). This context dependence extends the logic of cerebral preconditioning. Prior sublethal perturbations can alter the molecular response to later injury[7,8], and ischemic preconditioning can reshape the transcriptional architecture of the subsequent response rather than simply reduce its magnitude[9]. Although bacterial exposure should not be mechanistically equated with ischemic preconditioning, the conceptual parallel is informative. An earlier biological signal may exert its most important effect by changing the state from which a later challenge is interpreted.

Our experimental paradigms also show why the later challenge cannot be reduced to hypoxia intensity alone. SHX combined continuous HIF stabilization with nutrient restriction, whereas MHX incorporated repeated recovery periods in complete differentiation medium (Fig. 1A); the conditions therefore differed in duration, continuity and nutrient availability. $CoCl_2$-mediated HIF stabilization does not reproduce physiological oxygen deprivation, and its combination with glucose and pyruvate restriction therefore models selected components of metabolic stress rather than the full neurovascular environment of cerebral hypoperfusion. The two paradigms should thus be interpreted as distinct hypoxia-like metabolic stress trajectories rather than direct reproductions of in vivo hypoperfusion. This distinction is nevertheless relevant to vascular cognitive impairment and dementia (VCID), in which neural tissue

encounters heterogeneous and temporally evolving disturbances in perfusion, oxygen and metabolic support, with chronic cerebral hypoperfusion contributing to progressive dysfunction[41,42]. Our reductionist system does not reproduce this multicellular pathology. It instead isolates a principle relevant to prevention: intermittent metabolic instability may preserve an adaptive window in which prior biological inputs can still redirect the neuronal response, whereas continuous severe stress may exceed that capacity.

The microbiota–gut–brain axis provides a biologically relevant source of such prior inputs. Microbial communities and molecules influence the nervous system through immune, metabolic, endocrine and neural routes[12,13,43]. In cerebral ischemia, microbiota composition can modify experimental stroke outcome through gut–immune mechanisms, while microbiota-derived metabolites have also been implicated in inflammatory and repair responses after injury. These studies establish that microbial information can influence the response of the injured brain, but predominantly through systemic or neuroimmune routes. Our approach addresses a complementary question: whether a prior, controlled neuron–bacterium interaction can modify the subsequent intrinsic neuronal response to metabolic challenge in the absence of immune, vascular or intestinal intermediates.

Our previous work demonstrated that live *L. plantarum* can directly interact with neuronal cells and rapidly modulate calcium signaling, synaptic-associated proteins, and transcriptional activity[27]. In parallel, Jeong et al. (2024) showed that *L. plantarum* K8 lysates attenuate HIF1α accumulation and hypoxia-responsive gene expression in cellular models exposed to chemically induced hypoxic stress[28]. Importantly, bacterial lysates remained present during the hypoxic challenge in that study. Here, we extend these observations by showing that a preceding interaction with live bacteria, followed by a bacterial removal step, is associated with distinct neuronal responses to subsequent intermittent and continuous metabolic stress. The differential metabolic and transcriptional outcomes indicate that the consequences of microbial exposure depend on the trajectory of the later challenge rather than reflecting a uniform protective response. Although the persistence and molecular encoding of the initial bacterial influence remain to be established, these findings support a history-dependent framework for direct neuron–bacteria communication.

Transcriptomic profiling provided a molecular framework for this history-dependent response. Even without bacterial pre-exposure, MHX and SHX differed by 2,065 DEGs and remained distinct across hypoxia-, HIF1A- and chronic-hypoperfusion-related signatures (Fig. 2G–L; Suppl. Fig. S2D–F), confirming that they constitute distinct cellular states. Under SHX, ion-channel, synaptic-membrane and neuronal-signaling annotations were enriched despite pronounced structural disruption and reduced SYN1 expression. This may reflect compensatory signaling that was insufficient to preserve neuronal organization, or preferential persistence of particular stress-tolerant cell populations. MHX was instead enriched for cell-cycle regulation, DNA maintenance, chromosome organization and structural remodeling, consistent with a more dynamic transcriptional environment. Because differentiated B35 cells retain features of their neuroblastoma origin, these cell-cycle-associated signatures should be interpreted cautiously and cannot be taken as evidence of neuronal proliferation or regeneration. In the

context of the comparatively preserved cytoskeletal and neuritic organization observed under MHX, they are more conservatively interpreted as part of a broader cellular reorganization associated with the intermittent stress trajectory.

Against these distinct backgrounds, prior *L. plantarum* exposure produced its strongest functional and molecular effects after MHX. It increased the MTT signal under MHX but not SHX (Fig. 3B, C) and was associated with 167 versus 64 DEGs, respectively, with clearer bacteria-dependent sample segregation after intermittent stress (Fig. 3D–J; Suppl. Fig. S3). Under SHX, the response centered on metabolic, redox, proteostatic, autophagic and mitochondrial processes without improved metabolic viability, a pattern more consistent with residual stress management than coordinated neuronal rescue. Under MHX, bacterial pre-exposure engaged signaling, cytoskeletal, inflammatory and cell-death-related programs, including gene sets linked to negative regulation of intrinsic apoptotic signaling and oxidative-stress-induced cell death (Suppl. Figs. S4 and S5). These changes provide a plausible molecular context for the increased MTT signal but establish association, not a causal reduction in neuronal death. The response also encompassed synaptic-vesicle transport, exocytosis, growth-factor signaling, ion channels, neurotransmitter receptors and membrane functions, suggesting broader reorganization of neuronal communication. Measurements of calcium dynamics, membrane potential and electrophysiological activity will be required to determine how these transcriptional changes translate into neuronal function.

The global comparison reinforced the conditional nature of the bacterial effect. More than half of the DEGs distinguishing SHX from MHX were shared regardless of pre-exposure (Fig. 4A), showing that the subsequent stress trajectory remained the dominant determinant of the transcriptome. Yet synaptic, signaling, transport and cell-death-related genes were disproportionately represented among condition-specific responses, and bacterial pre-exposure increased rather than reduced transcriptional divergence between MHX and SHX (Fig. 4B, C). Only one DEG was shared between the bacterial responses detected under the two trajectories (Fig. 4D). The significance lies less in that locus than in the near absence of a conserved *L. plantarum*-responsive program. Biological resilience need not involve a universal set of “protective genes”; it may arise through different molecular configurations determined by the system’s history and current constraints[9,44–46].

This conditionality is especially relevant to the emerging study of direct neuron–bacteria communication[27,47]. Microbial signals are often described as though a metabolite or strain carries an intrinsic anti-inflammatory, neuroactive or protective instruction. Our findings support a more context-dependent interpretation. Bacterial exposure provides an initial input, the later metabolic challenge provides a second, and the final neuronal phenotype reflects their ordered interaction. This framework is consistent with models of the microbiota–brain axis that emphasize context and causality over fixed microorganism–phenotype associations[12], and it positions neuron–bacteria communication as a sequence of state transitions rather than isolated stimulus–response relationships.

An important question arising from these findings is which cellular mechanisms enable prior microbial interactions to influence subsequent neuronal responses. Bioelectrical signaling represents one potential mechanism through which environmental information may be integrated with cellular state and downstream gene regulation[48]. In neurons, membrane excitability and calcium-dependent signaling provide well-established links between electrical activity and transcriptional regulation, contributing to neuronal plasticity and adaptive responses[49,50]. Interestingly, the transcriptional programs associated with bacterial preconditioning in our study included genes involved in neurotransmitter signaling, membrane transport, and synaptic organization, suggesting that neuronal communication pathways may be sensitive to previous microbial exposure. Although these findings do not directly establish changes in membrane potential or neuronal electrical activity, they raise the possibility that bioelectrical mechanisms contribute to the integration of microbial signals with subsequent stress responses. Determining whether bacterial exposure induces measurable changes in neuronal bioelectrical state, and whether these changes influence responses to later environmental challenges, represents an important direction for understanding the mechanisms underlying history-dependent neuron–bacteria communication.

The different outcomes under MHX and SHX further suggest that bacterial preconditioning operates within a finite adaptive range. Classical cerebral preconditioning is similarly bounded: protective programs can increase tolerance to subsequent injury but may be overwhelmed when the later insult exceeds the system's compensatory capacity[8]. Importantly, SHX did not abolish bacterial-associated transcriptional responses altogether. Residual metabolic and proteostatic changes persisted but were not accompanied by improved MTT-derived viability. This dissociation suggests that cellular responsiveness and effective adaptation are not equivalent: a biological system may continue to react to environmental information after those responses are no longer sufficient to alter its functional trajectory.

The present findings also open several mechanistic questions. It remains to be determined which bacterial signals mediate preconditioning and whether their effects arise from membrane-associated interactions, secreted metabolites, or other products generated during the initial exposure. Bulk RNA sequencing also leaves unresolved whether the observed transcriptional changes reflect cell-intrinsic reprogramming, shifts in cellular subpopulations, or both. More fundamentally, identifying the cellular variables through which the influence of prior microbial exposure is maintained and subsequently affects the response to stress will provide a direct mechanistic basis for future studies.

Together, our results show that prior microbial exposure modifies the trajectory of a later neuronal stress response without predetermining its outcome. The effect remained functionally expressed within an intermittent, sublethal environment but became restricted under continuous severe stress. The broader implication is that the biological effect of a microbial signal cannot be inferred from the microorganism alone but emerges from its interaction with the subsequent environmental history of the receiving system. Defining these conditional relationships will be important for understanding the fundamental logic of neuron–bacteria communication and, ultimately, for identifying the conditions under which microbiota-derived signals can redirect vulnerable neuronal systems towards more adaptive trajectories.

Declarations

Declaration of generative AI and AI-assisted technologies in the manuscript preparation process

During the preparation of this work, the authors used ChatGPT (OpenAI) to assist with language editing, improve clarity and organization, and identify potential inconsistencies in the manuscript. The authors reviewed and edited the output as needed and take full responsibility for the content of the published article.

Competing interests:

Authors declare that they have no competing interests

Data and materials availability

Gene-level differential-expression lists used for the reported comparisons are provided in Annex Data S1–S4. Sequencing count matrices and additional information needed for reanalysis can be requested from the corresponding author.

Author Contribution

CH-R and AL-H conceived the study and developed the original conceptual framework. AL-H and JL-H performed the neuronal and bacterial experiments and analysed the data. AM-C and CJ-L contributed to the statistical analyses, data interpretation, and mathematical modelling. MTG-E and MPS-L contributed to the data interpretation, conceptual discussion and interdisciplinary interpretation of the results. JB-C and IR assisted with bacterial culture and microscopy experiments. CH-R, AL-H, JL-H, and S.G. wrote the original draft of the manuscript. All authors reviewed and revised the manuscript and approved its final version.

Acknowledgement

We thank Alejandro Vian, Jorge Trasobares, Jesús Merchán-Rubira and other members of Brain-Bacteria Interface (BBI) Lab for their fruitful comments on this research. This research was funded by the Spanish Ministry of Science and Innovation through PID2023-147361NA-I00 and the Ramón y Cajal program (RYC2020-029499-I, from the MICINN, FSE/ Agencia Estatal de Investigación) to C. H-R. The work has been funded also by the University of Turin (L.C) to A.L-H. We gratefully acknowledge support of the Spanish Ministry of Universities FPU Predoctoral Fellowship to J.L.-H. (FPU23/02273).

References

1. Lennon MJ, Sachdev PS (2026) Vascular cognitive impairment and dementia: Prevention, treatments, mechanisms and management options for the future. Neuropsychopharmacology: official publication Am Coll Neuropsychopharmacol. 10.1038/s41386-026-02331-3
2. Tian Z, Ji X, Liu J (2022) Neuroinflammation in Vascular Cognitive Impairment and Dementia: Current Evidence, Advances, and Prospects. Int J Mol Sci 23:6224
3. van der Flier WM et al (2018) Vascular cognitive impairment. Nat Rev Dis Primers 4:18003. 10.1038/nrdp.2018.3
4. Morgan AE, Mc Auley MT (2024) Vascular dementia: From pathobiology to emerging perspectives. Ageing Res Rev 96:102278. https://doi.org/10.1016/j.arr.2024.102278
5. Livingston G et al (2024) Dementia prevention, intervention, and care: 2024 report of the Lancet standing Commission. Lancet 404:572–628. 10.1016/s0140-6736(24)01296-0
6. Peng Y et al (2023) Current and future therapeutic strategies for Alzheimer's disease: an overview of drug development bottlenecks. Front Aging Neurosci 15:1206572. 10.3389/fnagi.2023.1206572
7. Dirnagl U, Becker K, Meisel A (2009) Preconditioning and tolerance against cerebral ischaemia: from experimental strategies to clinical use. Lancet Neurol 8:398–412. 10.1016/s1474-4422(09)70054-7
8. Gidday JM (2006) Cerebral preconditioning and ischaemic tolerance. Nat Rev Neurosci 7:437–448. 10.1038/nrn1927
9. Stenzel-Poore MP et al (2003) Effect of ischaemic preconditioning on genomic response to cerebral ischaemia: similarity to neuroprotective strategies in hibernation and hypoxia-tolerant states. Lancet 362:1028–1037. 10.1016/S0140-6736(03)14412-1
10. Amini M et al (2026) Synergistic Efficacy of Lactobacillus plantarum Supernatant-Preconditioned BM-MSCs in Alleviating Depression, Anxiety-Like Behavior, and Memory Impairment in a Rat Stress Model by Suppressing the NF-κB Pathway. Mol Neurobiol 63:405. 10.1007/s12035-025-05656-0
11. Cryan JF et al (2019) The Microbiota-Gut-Brain Axis. Physiol Rev 99:1877–2013. 10.1152/physrev.00018.2018
12. Cryan JF, Mazmanian SK (2022) Microbiota-brain axis: Context and causality. Sci (New York N Y) 376:938–939. 10.1126/science.abo4442
13. Needham BD, Kaddurah-Daouk R, Mazmanian SK (2020) Gut microbial molecules in behavioural and neurodegenerative conditions. Nat Rev Neurosci 21:717–731. 10.1038/s41583-020-00381-0
14. Cryan JF, Dinan TG (2012) Mind-altering microorganisms: the impact of the gut microbiota on brain and behaviour. Nat Rev Neurosci 13:701–712. 10.1038/nrn3346
15. Brusaferro A et al (2019) Gut dysbiosis and paediatric Crohn's disease. J Infect 78:1–7. 10.1016/j.jinf.2018.10.005
16. Tumani MF, Pavez C, Parada A (2020) Microbiota, hábitos alimentarios y dieta en enfermedad inflamatoria intestinal. Revista Chil de nutrición 47:822–829
17. Jia L et al (2025) Metagenomic analysis characterizes stage-specific gut microbiota in Alzheimer’s disease. Mol Psychiatry. 10.1038/s41380-025-02973-7

18. Li W et al (2025) The gut microbiota mediates memory impairment under high-altitude hypoxia via the gut–brain axis in mice. FEBS J 292:809–826. https://doi.org/10.1111/febs.17365
19. Wu JC (2012) Psychological Co-morbidity in Functional Gastrointestinal Disorders: Epidemiology, Mechanisms and Management. J Neurogastroenterol Motil 18:13–18. 10.5056/jnm.2012.18.1.13
20. Kern L, Mastandrea I, Melekhova A, Elinav E (2025) Mechanisms by which microbiome-derived metabolites exert their impacts on neurodegeneration. Cell Chem Biology 32:25–45. https://doi.org/10.1016/j.chembiol.2024.08.014
21. Dinan TG, Stanton C, Cryan JF (2013) Psychobiotics: a novel class of psychotropic. Biol Psychiatry 74:720–726. 10.1016/j.biopsych.2013.05.001
22. Ticinesi A et al (2018) Gut microbiota, cognitive frailty and dementia in older individuals: a systematic review. Clin Interv Aging 13:1497–1511. 10.2147/cia.S139163
23. Beltrán-Velasco AI, Reiriz M, Uceda S, Echeverry-Alzate V (2024) Lactiplantibacillus (Lactobacillus) plantarum as a Complementary Treatment to Improve Symptomatology in Neurodegenerative Disease: A Systematic Review of Open Access Literature. Int J Mol Sci 25. 10.3390/ijms25053010
24. Liu TH, Chiou J, Tsai TY (2016) Effects of Lactobacillus plantarum TWK10-Fermented Soymilk on Deoxycorticosterone Acetate-Salt-Induced Hypertension and Associated Dementia in Rats. Nutrients 8. 10.3390/nu8050260
25. Sittipo P, Choi J, Lee S, Lee YK (2022) The function of gut microbiota in immune-related neurological disorders: a review. J Neuroinflamm 19:154. 10.1186/s12974-022-02510-1
26. Wu Y et al (2022) Lactobacillus plantarum-derived postbiotics prevent Salmonella-induced neurological dysfunctions by modulating gut-brain axis in mice. Front Nutr 9:946096. 10.3389/fnut.2022.946096
27. Lombardo-Hernandez J et al (2025) An in vitro neurobacterial interface reveals direct modulation of neuronal function by gut bacteria. Sci Rep 15:25535. 10.1038/s41598-025-10382-7
28. Jeong J et al (2024) Lactiplantibacillus plantarum K8 lysates regulate hypoxia-induced gene expression. Sci Rep 14:6275. 10.1038/s41598-024-56958-7
29. Wu D, Yotnda P (2011) Induction and testing of hypoxia in cell culture. J Vis Exp. 10.3791/2899
30. Duly AMP, Kao FCL, Teo WS, Kavallaris M (2022) βIII-Tubulin Gene Regulation in Health and Disease. Front Cell Dev Biology 10–2022. 10.3389/fcell.2022.851542
31. Dong P, Li Q, Han H (2022) HIF–1α in cerebral ischemia (Review). Mol Med Rep 25. 10.3892/mmr.2021.12557
32. Iyalomhe O et al (2017) The Role of Hypoxia-Inducible Factor 1 in Mild Cognitive Impairment. Cell Mol Neurobiol 37:969–977. 10.1007/s10571-016-0440-6
33. Kim Y, Kim Y-J (2021) Effect of Obesity on Cognitive Impairment in Vascular Dementia Rat Model via BDNF-ERK-CREB Pathway. Biol Res Nurs 23:248–257. 10.1177/1099800420951633
34. Morè L et al (2022) CREB serine 133 is necessary for spatial cognitive flexibility and long-term potentiation. Neuropharmacology 219:109237. 10.1016/j.neuropharm.2022.109237

35. Naqvi S, Martin KJ, Arthur JS (2014) CREB phosphorylation at Ser133 regulates transcription via distinct mechanisms downstream of cAMP and MAPK signalling. Biochem J 458:469–479. 10.1042/bj20131115
36. Zhao H, Li Z, Wang Y, Zhang Q (2012) Hippocampal expression of synaptic structural proteins and phosphorylated cAMP response element-binding protein in a rat model of vascular dementia induced by chronic cerebral hypoperfusion. Neural Regen Res 7:821–826. 10.3969/j.issn.1673-5374.2012.11.004
37. Li YC, Kavalali ET (2017) Synaptic Vesicle-Recycling Machinery Components as Potential Therapeutic Targets. Pharmacol Rev 69:141–160. 10.1124/pr.116.013342
38. Marconcini L et al (1999) c- *fos-induced growth factor/vascular endothelial growth factor D induces angiogenesis < i > in vivo and in vitro. Proceedings of the National Academy of Sciences 96, 9671–9676, doi*:10.1073/pnas.96.17.9671
39. Müller JM, Krauss B, Kaltschmidt C, Baeuerle PA, Rupec RA (1997) Hypoxia Induces c- fos Transcription via a Mitogen-activated Protein Kinase-dependent Pathway *. J Biol Chem 272:23435–23439. 10.1074/jbc.272.37.23435
40. Jørgensen MB, Deckert J, Wright DC, Gehlert DR (1989) Delayed c-fos proto-oncogene expression in the rat hippocampus induced by transient global cerebral ischemia: an in situ hybridization study. Brain Res 484:393–398. 10.1016/0006-8993(89)90388-0
41. Anderle S, Dixon M, Quintela-Lopez T, Sideris-Lampretsas G, Attwell D (2025) The vascular contribution to cognitive decline in ageing and dementia. Nat Rev Neurosci 26:591–606. 10.1038/s41583-025-00950-1
42. Iadecola C (2013) The pathobiology of vascular dementia. Neuron 80:844–866. 10.1016/j.neuron.2013.10.008
43. Ohara TE, Hsiao EY (2025) Microbiota–neuroepithelial signalling across the gut–brain axis. Nat Rev Microbiol 23:371–384. 10.1038/s41579-024-01136-9
44. Marder E, Goaillard JM (2006) Variability, compensation and homeostasis in neuron and network function. Nat Rev Neurosci 7:563–574. 10.1038/nrn1949
45. Obrenovitch TP (2008) Molecular physiology of preconditioning-induced brain tolerance to ischemia. Physiol Rev 88:211–247. 10.1152/physrev.00039.2006
46. Vihervaara A, Duarte FM, Lis JT (2018) Molecular mechanisms driving transcriptional stress responses. Nat Rev Genet 19:385–397. 10.1038/s41576-018-0001-6
47. Rivero Guillén R (2026) Physical bacteria–neuron proximity and early cellular responses: a conceptual perspective. Front NeuroSci 20–2026. 10.3389/fnins.2026.1844325
48. Levin M (2021) Bioelectric signaling: Reprogrammable circuits underlying embryogenesis, regeneration, and cancer. Cell 184:1971–1989. 10.1016/j.cell.2021.02.034
49. Ma J, Chen Y, Wang Z, Wang R, Dong Y (2023) Lactiplantibacillus plantarum CR12 attenuates chronic unforeseeable mild stress induced anxiety and depression-like behaviors by modulating the gut microbiota-brain axis. J Funct Foods 107:105710. https://doi.org/10.1016/j.jff.2023.105710

50. Marom S, Marder E (2023) A biophysical perspective on the resilience of neuronal excitability across timescales. Nat Rev Neurosci 24:640–652. 10.1038/s41583-023-00730-9

Figures

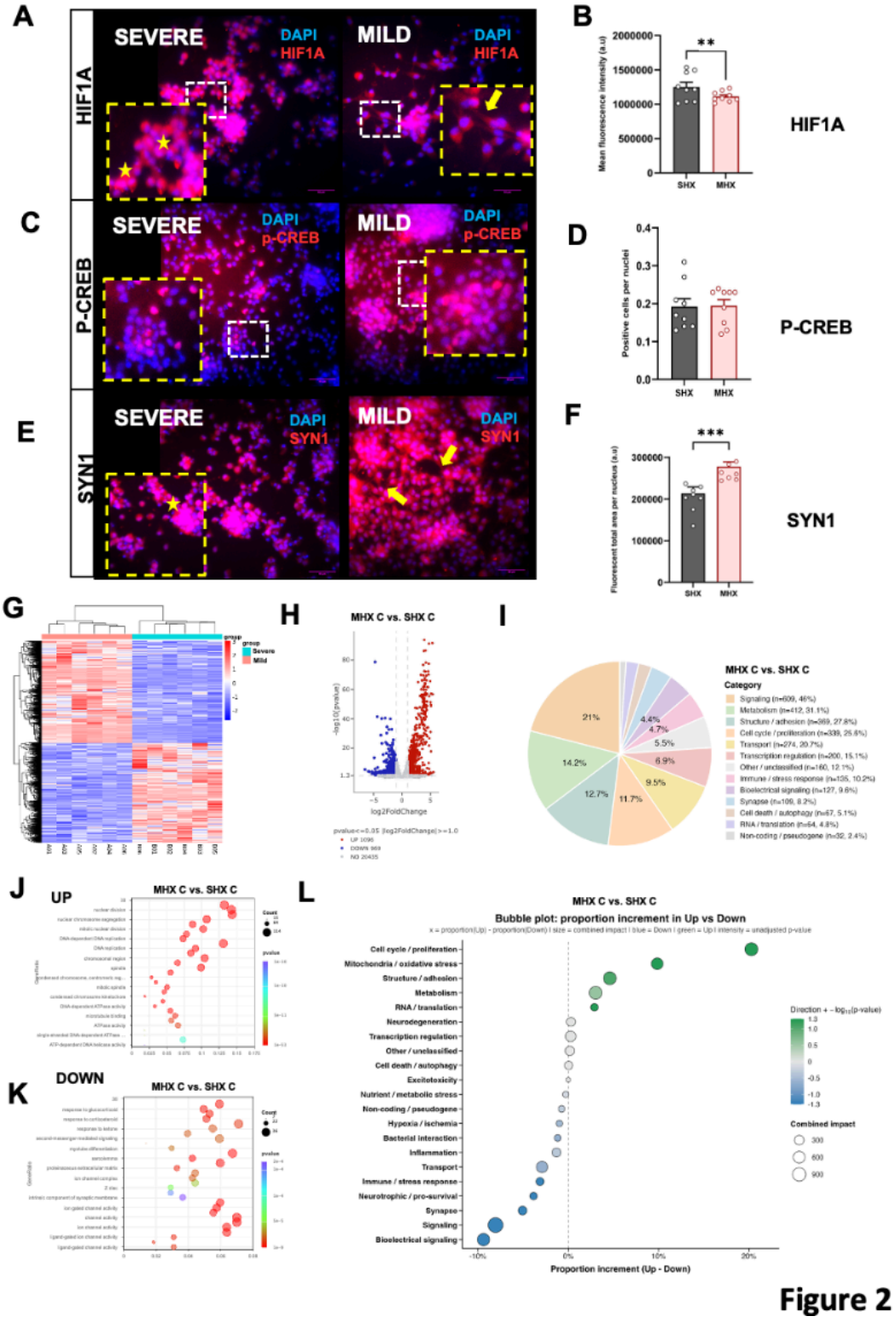


Figure 2

Figure 2

Morphological, Protein, and Transcriptional Characterization of Mild and Severe Hypoxia Phenotypes. (A–F) Morphologically, SHX neurons displayed a predominantly rounded shape, indicative of loss of cell adhesion (marked with yellow stars), as well as the presence of cell aggregates with diffuse neuronal interconnection. In contrast, the mild hypoxia group (MHX) displayed greater neuronal interconnection and higher cell density compared to SHX, with preserved neuritic extensions (marked with yellow arrows). (A, B) The severe hypoxia group (SHX) exhibited the highest levels of HIF1A expression analysed by mean fluorescence intensity. (C, D) Analysis of pCREB expression showed no significant differences between the MHX and SHX groups. (E, F) The synaptic marker SYN showed a significant reduction in expression in the SHX group in terms of fluorescence total area per nucleus. Data are presented as mean ± SEM. Statistical significance after population-averaged GEE analysis was set at $p < 0.05$, with levels of significance indicated as $p < 0.05$ (*),$p < 0.01$ (**), $p < 0.001$ (***), y $p < 0.0001$ (***). **(G)** Clustering analysis of the samples allowed the identification of two clearly differentiated groups corresponding to mild hypoxia (MHX) and severe hypoxia (SHX). **(H)** Volcano plot showing differential gene expression between intermittent mild (MHX) and continuous severe (SHX) hypoxia-like stress conditions. A total of 2,065 genes met the predefined differential-expression thresholds ($|\log_2 FC| \geq 1$, $p \leq 0.05$), including 1,096 upregulated and 969 downregulated genes in MHX relative to SHX. **(I)** Pie chart showing the distribution of DEGs across major biological categories. Each percentage represents the contribution of each category relative to the total number of annotated DEGs. **(J-K)**Functional enrichment analysis (Gene Ontology) indicated that the MHX phenotype is predominantly associated with processes related to cell proliferation and structural maintenance, whereas the SHX phenotype showed a higher representation of genes linked to the loss of functions related to neuronal communication and plasticity. **(L)** Bubble plot summarizing differences in the proportions of upregulated and downregulated genes across functional categories. The analysis revealed a greater representation of cell cycle and proliferation-related genes among those upregulated in MHX, alongside a lower representation of signaling and synaptic categories. The x-axis represents the difference in proportions (Up − Down). Bubble color indicates statistical significance based on the functional-category comparisons described in Methods, while bubble size reflects impact, calculated as the cumulative sum of $\log_2$fold-change values. Genes included in this analysis met the predefined differential-expression thresholds ($|\log_2 FC| \geq 1$, $p \leq 0.05$).

Supplementary Files

This is a list of supplementary files associated with this preprint. Click to download.

- LeanoHinojosaSupplementaryMaterialsFINALrevisado.docx